AFRL-RW-EG-TP-2016-002

Example Problems in LES Combustion

Douglas V. Nance

Air Force Research Laboratory
Munitions Directorate/Ordnance Division
Lethality, Vulnerability and Survivability Branch
(AFRL/RWML)
Eglin AFB, FL 32542-5910

September 2016

AIR FORCE RESEARCH LABORATORY
MUNITIONS DIRECTORATE

■ Air Force Materiel Command ■ United States Air Force ■ Eglin Air Force Base, FL 32542

REPORT DOCUMENTATION PAGE

Form Approved
OMB No. 0704-0188

1. REPORT DATE *(DD-MM-YYYY)*	2. REPORT TYPE	3. DATES COVERED *(From - To)*
26-09-2016	Technical Memorandum	

4. TITLE AND SUBTITLE

Example Problem in LES Combustion

5a. CONTRACT NUMBER

5b. GRANT NUMBER

5c. PROGRAM ELEMENT NUMBER

6. AUTHOR(S)

Douglas V. Nance

5d. PROJECT NUMBER

5e. TASK NUMBER

5f. WORK UNIT NUMBER
W0TP

7. PERFORMING ORGANIZATION NAME(S) AND ADDRESS(ES)

Air Force Research Laboratory, Munitions Directorate
Ordnance Division
Lethality, Vulnerability, and Survivability Branch (AFRL/RWML)
Eglin AFB FL 32542-6810

8. PERFORMING ORGANIZATION REPORT NUMBER

AFRL-RW-EG-TP-2016-002

9. SPONSORING / MONITORING AGENCY NAME(S) AND ADDRESS(ES)
Air Force Research Laboratory, Munitions Directorate
Ordnance Division
Lethality, Vulnerability, and Survivability Branch (AFRL/RWML)
Eglin AFB FL 32542-6810
Technical Advisor: Kirk J. Vanden, PhD

10. SPONSOR/MONITOR'S ACRONYM(S)

11. SPONSOR/MONITOR'S REPORT

AFRL-RW-EG-TP-2016-002

12. DISTRIBUTION / AVAILABILITY STATEMENT

Distribution A: Approved for public release; distribution unlimited. Approval Confirmation 96W-2016-0160

13. SUPPLEMENTARY NOTES

14. ABSTRACT

This memorandum provides a brief introduction to finite rate chemistry in the framework of large eddy simulation for compressible flow fields. Particular emphasis is placed upon the filtered reaction rate expression through the use turbulent chemical closure terms. The Eddy Break-Up model is an example of this type of closure term. Within the multiphase physics computer code LESLIE3D, these algorithms are tested on a gas phase acetylene combustion problem and on a shock wave initiated droplet evaporation and combustion problem. Results are shown for each problem. Comparisons are shown for kinetic and Eddy Break-Up model filtered reaction rates. For the droplet problem, droplet evaporation, combustion and product formation is demonstrated.

15. SUBJECT TERMS
Combustion, LES, Large Eddy Simulation, Kerosene, turbulence, droplets

16. SECURITY CLASSIFICATION OF:			17. LIMITATION OF ABSTRACT	18. NUMBER OF PAGES	19a. NAME OF RESPONSIBLE PERSON
a. REPORT	b. ABSTRACT	c. THIS PAGE			Pedro A. Lopez-Fernandez
UNCLASSIFIED	UNCLASSIFIED	UNCLASSIFIED	SAR	36	19b. TELEPHONE NUMBER *(include area code)* 850-883-2707

Standard Form 298 (Rev. 8-98)
Prescribed by ANSI Std. Z39.18

This page intentionally left blank

TABLE OF CONTENTS

LIST OF FIGURES

1.0 INTRODUCTION

This memorandum addresses issues involving gas-phase finite rate chemistry and droplet vaporization as simulated by the LESLIE3D computer program. LESLIE3D is an acronym for Large Eddy Simulation with LInear Eddy model in 3 Dimension and is developed by Professor Suresh Menon at the Georgia Institute of Technology. Although this computer program is the product of ongoing research, it is adept at simulating the multiphase physics of mixtures of gases with particles or droplets. Finite rate chemical reaction mechanisms are incorporated within this computer program for an arbitrary number of species and reactions (constrained only by available computer memory). LESLIE3D has powerful capabilities for the simulation of gas phase chemistry. Surface chemistry for solid particles is also an inherent capability of the code, e.g., the combustion of Aluminum particles. Simulation of the evaporation and subsequent heating and combustion of liquid droplets is a historical, organic capability for this computer program. These algorithms spring from one of LESLIE3D's primary development efforts, the simulation of turbulent flow and chemistry in gas turbine combustors.

1.1 Core LESLIE3D Algorithms

No discussion of LESLIE3D is complete without a brief exposition of LESLIE3D's core numerical algorithms. Although there are many algorithms undergirding the code's representation of continuum dynamics, three major algorithms stand out from the others. First, LESLIE3D has state-of-the-art capabilities for the Large Eddy Simulation (LES) of compressible turbulence. Suresh Menon's Locally Dynamic subgrid Kinetic energy Model (LDKM) is directly incorporated in the code.[1] To review, the idea behind LES is simple. Organized fluid motions can be ordered in terms of scale, large size eddies cascading down to small size eddies. Informally, LES establishes a line of demarcation between the large and small scales.[2] Eddies within the large range of scales are resolved numerically by solving the filtered Navier-Stokes equations.[3] The properties of small scale eddies are determined by modeling. The assumption implicitly made is that at the small scales, turbulent motions are universal.[4] Various mathematical models are used to compute the small scale (subgrid) properties based upon properties of the main flow in time. As its principal driver, LDKM exploits the similarity between the Leonard stress tensor at the so-called test scale with the subgrid scale stress tensor. On the axis of turbulent scales, the test scale is a finite locus of scales that are both numerically resolved and modeled. Without getting into the

mathematical details, similarity between these two scales requires use of the subgrid and subtest scale kinetic energy for the turbulence. From non-zero initial values, the behavior of subgrid kinetic energy is described by an evolution equation that is included in the system of governing equations.[4] This combination of numerical simulation and modeling culminates in the production of time and space-dependent coefficients for the production and dissipation of turbulence in space. Hence, LDKM is truly a local LES model.

The second major capability of LESLIE3D is its capacity for capturing the physics of shock-turbulence. Shock waves are most often modeled as discontinuities in the flow field. That is to say, across the shock wave front, flow properties such as pressure, density, temperature, entropy and individual velocity components change abruptly. The Euler equations, a truncated set of Navier-Stokes equations (disregarding viscous effects), are often used to model shock waves since the Euler equations admit discontinuous solutions. Unfortunately, discontinuous solutions are not admitted by the Navier-Stokes equations. Even for tiny regions near the shock front, solutions must be smooth. In order to automatically resolve shock waves, the use of upwind or asymmetrical differencing is required.[5] On the other hand, to resolve turbulence, centered or symmetrical differencing is required. This situation presents a dilemma. The asymmetrical stencils required for shock wave resolution possess a great deal of numerical viscosity; the associated dissipation tends to damp subtle turbulent fluctuations from the flow field. Conversely, the simulation of turbulence favors the use of symmetric, high order computational stencils. By design, symmetric (or centered) stencils incorporate information from both directions defined by the stencil. For shocked flow fields, the bidirectional incorporation of information induces instability in the shock wave solver. The instability manifests itself in violent oscillations of flow field properties originating near the shock locus and spreading outward. These oscillations ultimately corrupt the numerical solution, induce instability and cause it to diverge.

LESLIE3D remedies this dilemma in two ways. First, we draw upon the mathematics of the Piece-wise Parabolic Method (PPM) to implement a very low dissipation shock-capturing scheme.[6] The reconstruction process mimics the “flattening” procedure used by PPM to limit the amount of dissipation used to grant a smooth shock solution. A variant of the Harten, Lax and van Leer Contact-preserving shock-capturing scheme is employed along with the Einfeld correction method for carbuncle instabilities (HLLC/E).[7,8] For the preservation of turbulent fluctuations, this scheme performs on par with PPM. The second and somewhat more complex

algorithm implemented for shock-turbulence capture is referred to as the “hybrid” scheme. The hybrid scheme utilizes a “switch” to apply HLLC/E in the neighborhood of shock waves and a high order centered MacCormack scheme in smooth regions of the flow field. This method performs quite well and has been validated in number of studies.[4]

The third major capability for LESLIE3D is provided by Lagrangian particle/droplet tracking algorithms for both diffuse and dense dispersed phases. These particle methods are fully coupled with the gas phase to provide for the highly accurate simulation of fuel combustor flow fields. In its original incarnation, LESLIE3D could only simulate diffuse particle fields where the particle volume fraction is rather small. In recent years, the dispersed field algorithms have been upgraded to address dense collections of particles.[9] The difference lies in the fact that dense particle fields exert an internal “pressure” on themselves. Particles or droplets entrained in diffuse fields are not subjected to this pressure. For dense dispersed fields, this pressure is very important in determining the forces exerted on particles. This inter-particle force is not found in diffuse fields. Instead, diffuse fields do include the drag force. This force is determined through the use of empirical drag laws.[10]

The information presented above provides only the briefest introduction to some of LESLIE3D’s capabilities from the viewpoint of physics, not computer programming. In the discussions that follow, we focus on LESLIE3D’s turbulent, finite rate chemistry algorithms. These algorithms accurately capture gas phase reaction kinetics, but more importantly, the physics of turbulent mixing is also accurately represented. It is very important to understand that for turbulent flow fields, if the turbulent motions are not accurately simulated, the rates for chemical reactions are incorrectly computed, and inaccurate numerical solutions result.

1.2 Combustion of Vapor Clouds

A class of scenarios generating widespread engineering interest involves the combustion of a cloud of vapor released into the atmosphere.[11,12] For our purposes, the constituents of cloud may be thought of in the classical sense of combustion. That is to say, the cloud is composed of the fuel (a combustible chemical, something that likes to give up electrons) and the oxidizer (a substance that likes to accept electrons). Combustible fuels always present safety concerns. These fuels are usually stored in tanks (either above or below ground), and given that many of these tanks are quite large and can store a great deal of chemical energy. It must also be realized that this type

of fuel only burns when in the gas phase. Before a liquid fuel can burn, it must first vaporize. Note that a partially filled liquid fuel tank contains an ullage volume (a void space above the surface of the liquid fuel volume). If this tank is heated (even by the sun), part of the fuel may vaporize into the ullage volume and subsequently pressurize the tank. A relief valve or vent installed on the tank can vent fuel vapor into the atmosphere and present a combustion hazard. If no such valve is present, then it is possible that the over pressurized tank may rupture releasing large amounts of fuel into the surroundings. This scenario constitutes a significant combustion hazard. If ignited by some random circumstance, then the fuel may begin to burn atomizing and vaporizing more fuel. If unchecked, this combustion process can cascade into a deflagration or detonation. Note also that light hydrocarbon fuels. e.g., acetylene and propane exist as gases at room temperature, so they are ready to combust if initiated. For these reasons, the combustion of fuel vapor clouds deserves study in the interest of engineering safer fuel storage and handling systems. Illustrating some aspects of the study is the focus of this memorandum with a particular emphasis on turbulent chemistry.

2.0 Technical Aspects of Turbulent, Gas Phase Combustion

This memorandum is fundamental in that it focuses on gas phase chemistry in a turbulent (and in some cases) shocked flow environment. Gas phase chemistry is exclusively considered in order to establish the physical framework for chemical reactions. The involvement of fuel droplets along with fuel atomization and evaporation is also very important, but these multiphase processes inevitably lead to the fundamental process of gas phase combustion.

2.1 Finite Rate Chemical Mechanisms

A finite rate chemical mechanism consists of a set of distinct chemical reactions involving a set of chemical species. The term “finite rate” is used because each chemical reaction requires a finite, non-zero amount of time to run to completion. For this simple example, the chemical species are identified as compounds or elements. Consider the combustion of acetylene gas. Acetylene (C_2H_2) is a simple hydrocarbon fuel characterized as an alkyne since the Carbon atoms are joined by a triple covalent bond. A diagram of this molecule is shown in Figure 1.

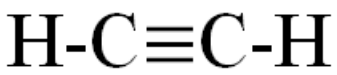

Figure 1. Molecular Structure of Acetylene

Acetylene is quite reactive due to the presence of the triple bond since this bond implies that three pairs of electrons are being shared between the Carbon atoms. Carbon has four electrons in its outer shell. Since it would like to complete this shell, it would like to share four other electrons. It does so, in this case, by sharing three electrons with its neighboring Carbon, and one electron with the nearest Hydrogen atom. The electron cloud formed by the shared electrons of the triple bond is an irresistible temptation for Oxygen, an element that loves to acquire electrons. The fundamental combustion reaction for acetylene can be written as follows.

$$C_2H_2 + 5/2\ O_2 \rightarrow 2\ CO_2 + H_2O \qquad (2.1.1)$$

For those who may not be familiar with chemical reaction equations, the species listed on the left side of the equation are called reactants; the species occurring on the right side of the equation are called products. Complete combustion, as implied by Equation (2.1.1), does not occur in reality. In truth, other chemical products are formed in small quantities, especially when a disproportionate amount of fuel is available compared with oxidizer. Still, acetylene is a very light hydrocarbon (molecular weight 26.02 g/mol), so with a preponderance of oxygen, we expect a high level of conversion into the products specified by (2.1.1). The coefficients (1, 5/2, 2 and 1) shown for the species in (2.1.1) are termed as stoichiometric coefficients. Although these coefficients are easily interpreted as dimensionless quantities, they in fact have the dimension of molecules (a cardinal number) or in groups as moles. Recall that a mole contains Avogardro's number of (6.023×10^{23}) molecules. In this light, one mole of acetylene can combust with 5/2 moles of oxygen gas to produce two moles of Carbon dioxide and one mole of water vapor. Of course, realistic problems involve scalar multiples of (2.1.1).

Equation (2.1.1) represents a static concept; it confers no information on the rate at which the reaction progresses. Rate information is provided, in one view, by the conventional theory of chemical kinetics. In a more general case, reactions such as (2.1.1) have both forward (r_f) and backward (r_b) rates.[13] These rates may be formulated as follows:

$$r_f = k_f\,[C_2\,H_2]^{R1}\,[O_2]^{R2} \qquad (2.1.2)$$

$$r_b = k_b\,[CO_2]^{P1}\,[H_2O]^{P2} \qquad (2.1.3)$$

Parameters k_f and k_b are the forward and backward rate coefficients. The square bracket notation [ ] indicates a measure of concentration, generally moles per cubic centimeter (mol/cm^3). The parameters R_1, R_2, P_1 and P_2 are exponents for the concentration factors. Under the conventional theory, these parameters along with components of the rate coefficients must be determined from laboratory experiments. More specifically, special curve fitting routines are required. Often, as a first approximation, these exponents are chosen as the matching stoichiometric coefficients. But for more detailed calibrations of the kinetics, widely different values are chose for these exponents. The general form for a rate coefficient may be written as

$$k = AT^n \exp\left(-\frac{E_a}{RT}\right) \qquad (2.1.4)$$

Equation (2.1.4) is cast in Arrhenius form, an approximation of the potential energy surface for the reaction. Specifically, A is denoted as the pre-exponential factor; T is the absolute temperature, and E_a is the activation energy.[13] The activation energy is the "height" of the potential energy barrier that must be overcome for the reaction to proceed. On inspection, (2.1.4) is intuitive; note that for higher values of the activation energy, the reaction rate is reduced. Higher temperatures are required to compensate for the increase in E_a. Also, for exothermic (energy liberating) reactions such as acetylene combustion, the reaction rate is proportional to temperature, so an increase in temperature elevates the reaction rate. The final term in (2.1.4), R, is the universal gas constant.

As it happens, for acetylene combustion, the backward rate is quite small, so we consider only the forward reaction (2.1.1) with the rate (2.1.2). The data required by (2.1.4) is provided in Table 1.

Table 1. Arrhenius Rate Coefficient Data for Single-Step Acetylene Combustion

A (mol/cm^3/s)	E_a (kcal/mol)	X_1	X_2
6.5×10^{12}	30	0.5	1.25

This acetylene reaction kinetics model and data is used for an example problem presented later in this memorandum.

2.2 The Closure Problem for Turbulent Chemistry

The Locally Dynamic subgrid Kinetic energy Model (LDKM) evolves from the filtered Navier-Stokes equations.[4] As a result, new terms appear in the equations; these terms involve averages of moments of flow properties. This mathematical process differs from the classical Reynolds Averaging method to some degree as it establishes the requisite separation in scales of motion. These new terms have the effect of adding variables to the system of equations so that the total number of variables exceeds the total number of equations. At face value, this system is unsolvable; hence, the *closure problem* results. It is necessary to add equations to the system and achieve mathematical closure. For the purposes of this work, we consider only the species evolution equation, i.e.,

$$\frac{\partial \bar{\rho}\tilde{Y}_k}{\partial t} + \frac{\partial}{\partial x_i}\left[\bar{\rho}\left(\tilde{Y}_k\tilde{u}_i + \widetilde{Y_k}\tilde{V}_{i,k}\right) + Y_{i,k}^{sgs} + \theta_{i,k}^{sgs}\right] = \dot{\bar{\omega}}_k \qquad (2.2.1)$$

In this equation, ρ is the local density for the species mixture; Y_k is the mass fraction of species k, and the $V_{i,k}$ are diffusion velocity components for the k^{th} species. Specifically, the filtered version of this expression is

$$\tilde{V}_{i,k} = -\frac{\bar{D}_k}{\tilde{Y}_k}\frac{\partial \tilde{Y}_k}{\partial x_i} \qquad (2.2.2)$$

where D_k is the diffusion coefficient for species k. The terms added by the filtering process are $Y_{i,k}^{sgs}$, $\theta_{i,k}^{sgs}$ and in another sense, $\dot{\bar{\omega}}_k$, the filtered reaction rate. The first two terms are the subgrid convective species flux $Y_{i,k}^{sgs}$ and the subgrid diffusive species flux $\theta_{i,k}^{sgs}$. The formal expressions for these terms are

$$Y_{i,k}^{sgs} = \bar{\rho}_g\left(\langle u_i Y_k\rangle - \tilde{u}_i\tilde{Y}_k\right) \qquad (2.2.3)$$

$$\theta_{i,k}^{sgs} = \bar{\rho}\left(\langle V_{i,k}Y_k\rangle - \tilde{V}_{i,k}\tilde{Y}_k\right) \qquad (2.2.4)$$

In (2.2.3) and (2.2.4), the angle brackets indicate the same mass-average denoted by the ~ symbol. In practice, the subgrid convective species flux is modeled; on the other hand, the subgrid diffusive species flux is neglected as it is thought to be small compared to other terms. The more critical term for turbulent chemistry is the filtered reaction rate. For this term, the Eddy Break-Up (EBU) model, a simple turbulent closure, is applied.[14]

The EBU model compares two separate reaction rates, first, the kinetic rate produced by the chemical mechanism and second, a mixing rate that takes turbulent motions into account. For the latter rate, the mixing time scale is defined as

$$\tau_{\text{mix}} = \frac{\text{CEBU}\cdot\Delta t}{\sqrt{2k^{\text{sgs}}}} \tag{2.2.5}$$

In this equation, CEBU is constant, usually set at one. The solution time step is Δt, and k_{sgs} is the space and time dependent subgrid kinetic energy determined by the evolution equation

$$\begin{aligned}\frac{\partial}{\partial t}(\bar{\rho}k^{\text{sgs}}) + \frac{\partial}{\partial x_i}(\bar{\rho}\tilde{u}_i k^{\text{sgs}}) \;=\; & \frac{\partial}{\partial x_i}\left[(\bar{\rho}\nu_t \;+\; \mu)\frac{\partial k^{\text{sgs}}}{\partial x_i} \;+\; \frac{\bar{\rho}\nu_t\tilde{R}}{\text{Pr}_t}\frac{\partial\tilde{T}}{\partial x_i}\right] \\ & -\left(1 \;+\; \alpha_{pd}\left(M_t^{sgs}\right)^2\left\{\frac{\bar{\rho}\tilde{S}k^{\text{sgs}}}{D_{k^{\text{sgs}}}}\right\}^2\right)\left(\tau_{ij}^{\text{sgs}}\frac{\partial\tilde{u}_j}{\partial x_i} \;+\; \bar{\rho}c_\varepsilon\frac{(k^{sgs})^{3/2}}{\bar{\Delta}}\right)\end{aligned} \tag{2.2.6}$$

Equation (2.2.6) is integrated along with the governing Navier-Stokes equations. The turbulent mixing rate is inversely proportional to this mixing time by a factor related to the driving stoichiometric coefficients. The EBU reaction rate is chosen as the minimum of the kinetic and turbulent mixing reaction rates. In most cases, the magnitude of the kinetic rate far exceeds the turbulent rate. If the kinetic rate is applied in turbulent flow simulations, the chemical reaction rates are over predicted by a significant margin. The classical EBU model differs from LESLIE3D's model, and the differences are worthy of a brief description. The main assumption behind EBU is that chemistry does not play an explicit role; instead, turbulent motions govern the reaction rate. In this realization, the gas phase reaction zone is comprised of volumes of both unburned and burned gases mixed by turbulent eddies. The average reaction rate is directly proportional to the level of temperature fluctuations and inversely proportional to a turbulence time scale. The level of temperature fluctuations is given, in part, by the expression

$$\Theta = \frac{T - T_1}{T_2 - T_1} \tag{2.2.7}$$

as is based upon laminar flame theory [15] where

$$T_2 = T_1 + \frac{QY_F}{C_P} \tag{2.2.8}$$

In these formulas, Q is the chemical energy liberated by the combustion reaction; Y_F is the mass fraction of fuel, and C_p is the mixture constant pressure specific heat. On the other hand, the classical EBU time scale is modeled as

$$\tau_{\mathrm{EBU}} = \frac{k}{\varepsilon} \tag{2.2.9}$$

where k and ε are the kinetic energy and energy dissipation rate for the turbulence. With the use of these quantities, the classical EBU reaction rate is defined as

$$\dot{\omega}_{\Theta} = C_{\mathrm{EBU}}\bar{\rho}\frac{\varepsilon}{k}\tilde{\Theta}\left(1-\tilde{\Theta}\right) \tag{2.2.10}$$

In this equation, $\bar{\rho}$ is the mixture density and the tilde symbol indicates an average. Of course, C_{EBU} is a constant chosen for the model. LESLIE3D's EBU model is implemented differently. An EBU reaction rate is computed for each reaction. All of the species used in the problem (reactants and products) are concatenated in order. If a particular species is a product (non-zero stoichiometric coefficient P_j), then set

$$\mathrm{P} = \min\left(\mathrm{P}, \frac{Y(\mathrm{P}_j)}{\mathrm{P}_j}\right) \tag{2.2.11}$$

A special caveat on (2.2.11) is that if the kinetic rate for the reaction goes forward, then it depends solely on reactant concentrations, so we set P equal zero. Conversely, if the species is a reactant (non-zero stoichiometric coefficient R_j), we set

$$R = \min\left(R, \frac{Y(\mathrm{R}_j)}{\mathrm{R}_j}\right) \tag{2.2.12}$$

If the reaction proceeds in the reverse direction, it depends solely on the product concentrations, so R is set to zero in this case. With the use of these details, the LESLIE3D EBU reaction rate is computed as

$$\dot{\omega} = \frac{P-R}{\tau_{\mathrm{mix}}} \tag{2.2.13}$$

for the reaction in question. The EBU model, in either of the forms shown here, is an effective and relatively inexpensive closure for turbulent chemistry. Other methods certainly exist since closures are, in fact, models.

2.3 Initializing the Turbulent Field

Although Menon's LDKM methodology constitutes a state-of-the-art model, the subgrid kinetic energy equation is an evolution equation that requires a non-zero initial turbulent velocity and subgrid kinetic energy field in order to simulate the evolution of the turbulence. For any three-dimensional volume, there are an infinite number of possible turbulent velocity distributions; we must select one such distribution for initializing LESLIE3D. For problems involving shock waves, we may define a non-zero velocity and subgrid kinetic energy field at the shock wave outflow.

Since the resolved velocity field is non-zero, the turbulence cannot decay before the simulation begins. This idea is rather *ad hoc* since we do not know *a priori* the turbulence velocity field in this region. For problems involving initially stagnant (zero velocity), shock-free flow fields, the aforementioned procedure does not apply. Instead, one must define a field of isotropic turbulence consistent with the governing equations in the ambient gas volume. For even non-shocked flow fields, this turbulence can evolve for many solution iterations without decaying, and it is completely physical. Moreover, this field is defined strictly in terms of three-dimensional, resolved field velocity components; the subgrid kinetic energy is initialized consistent with the resulting flow field kinetic energy. Below, the mathematical methodology is described for initializing the initial turbulent velocity field.[16]

Begin by considering a nearly quiescent flow field with velocity field $\vec{v} = \vec{v}(x_1, x_2, x_3)$. For the flow field to be incompressible, we require that $\nabla \cdot \vec{v} = 0$. By performing a Fourier integral transform on this equation, one obtains

$$\breve{\vec{v}} \cdot \vec{k} = 0 \tag{2.3.1}$$

where the wavevector is defined as

$$\vec{k} = \left(k_x, k_y, k_z\right) \tag{2.3.2}$$

The transformed variables are indicated by the $\breve{}$ symbol. With (2.3.1) in mind, suppose that we start with a more general velocity field $\vec{v}$ where (2.3.1) does not hold true. It is necessary to alter this velocity field so that (2.3.1) does hold. For the general $\vec{v}$, its multi-dimensional Fourier transform may be written as follows.

$$\breve{\vec{v}} \;=\; \breve{\vec{v}}_{||\vec{k}} \;+\; \breve{\vec{v}}_{\underline{|}\,\vec{k}} \tag{2.3.3}$$

Since (2.3.3) is tediously annotated, what this equation really says is that a the Fourier transformation of a general velocity field can be decomposed into the sum of velocity fields parallel and perpendicular to wavevector $\vec{k}$. From what this equation says, in the light of (2.3.1), the velocity field that we need is the one perpendicular to $\vec{k}$, so we solve (2.3.3) for this part of the transformed velocity field, i.e.,

$$\breve{\vec{v}}_{\underline{|}\,\vec{k}} \;=\; \breve{\vec{v}} \;-\; \breve{\vec{v}}_{||\vec{k}} \tag{2.3.4}$$

Observing the sense of the vector $\vec{k}$, we note that $\breve{\vec{v}}_{||\vec{k}}$ is that component of $\breve{\vec{v}}$ in the direction of the unit vector $\hat{k}$ where

$$\hat{k} = \frac{\vec{k}}{\|\vec{k}\|} = \frac{\vec{k}}{k} \tag{2.3.5}$$

Hence,

$$\breve{\vec{v}}_{||\vec{k}} = \frac{\vec{k}}{k}\left(\breve{\vec{v}} \cdot \frac{\vec{k}}{k}\right) = \frac{\vec{k}}{k^2}\left(\breve{\vec{v}} \cdot \vec{k}\right) \tag{2.3.6}$$

By substituting into (2.3.4), we obtain

$$\breve{\vec{v}}_{\underline{|}\,\vec{k}} = \breve{\vec{v}} - \frac{\vec{k}}{k^2}\left(\breve{\vec{v}} \cdot \vec{k}\right) \tag{2.3.7}$$

For computational purposes, it is useful to rewrite (2.3.7) in indicial notation where

$$\breve{v}_{i\,\underline{|}\,\vec{k}} = \breve{v}_i - \frac{k_i}{k^2}\left(\breve{v}_j k_j\right) = \left(\delta_{ij} - \frac{k_i k_j}{k^2}\right)\breve{v}_j \tag{2.3.8}$$

Equation (2.3.8) is the formula needed to create an incompressible velocity field from an arbitrary non-conservative velocity field.

To compute the incompressible velocity field, as mentioned above, we start with an arbitrary velocity distribution produced by using a pseudorandom number generator to create the velocity components.[17] In this case, the magnitude of each random velocity vector is kept fairly small. The next step is to perform a discrete Fourier transform on this velocity field. Each block in the computational flow field is fully structured; that is, each point in the grid is indexed by the ordered triple (i, j, k) where $1 \le i \le$ imax, $1 \le j \le$ jmax and $1 \le k \le$ kmax. To support the loop structure of the transform, it is helpful to require that imax, jmax and kmax be odd natural numbers. Then, the field cell counts in the index directions become

$$\begin{aligned} \text{icmax} &= \text{imax} - 1 \\ \text{jcmax} &= \text{jmax} - 1 \\ \text{kcmax} &= \text{kmax} - 1 \end{aligned} \tag{2.3.9}$$

The counting index maxima for the transform become

$$\begin{aligned} N_1 &= \text{icmax}/2 \\ N_2 &= \text{jcmax}/2 \\ N_3 &= \text{kcmax}/2 \end{aligned} \tag{2.3.10}$$

Let the velocity vector be denoted as

$$\vec{v} = (u_1, u_2, u_3) \tag{2.3.11}$$

then the forward transform may be written as

$$\breve{u}_p(k_1, k_2, k_3) = \sum_{n_1=1}^{N_1-1}\sum_{n_2=1}^{N_2-1}\sum_{n_3=1}^{N_3-1} u_p(n_1, n_2, n_3)\exp[-i(k_1 n_1 + k_2 n_2 + k_3 n_3)] \tag{2.3.12}$$

where $1 - N_p/2 \ \leq \ k_p \ \leq \ N_p/2,\ p$ =1, 2, 3. As a matter of review, (2.3.12) relies upon the Euler formula

$$\exp(i\theta) \ = \ \cos(\theta) + i\,\sin(\theta) \tag{2.3.13}$$

Note that the *i* in (2.3.12) is the imaginary unit. Moreover, the computed Fourier coefficients $\hat{u}_p$ are complex numbers. That is to say, while the velocity components u_p are numbers on the real line, the Fourier coefficients $\hat{u}_p$ exist in the complex plane. These coefficients are ready for the incompressibility correction.

The correction of the $\breve{u}_p$ to enforce incompressibility (more pertinently, mass conservation), is implemented in the same three nested loops implied by the transform (2.2.12). Instead of this transform, equation (2.3.8) is calculated. In pseudo-code, the loops may be expressed as follows.

For$1 - N_1/2 \leq k_1 \leq N_1/2$,$1 - N_2/2 \leq k_2 \leq N_2/2$,$1 - N_3/2 \leq k_3 \leq N_3/2$, with $k_p \neq 0$, for all $p = 1,2,3$, we compute

$$\mathrm{Re}\left(\vec{\breve{v}} \cdot \vec{k}\right) = \mathrm{Re}(\breve{u}_1)k_1 + \mathrm{Re}(\breve{u}_2)k_2 + \mathrm{Re}(\breve{u}_3)k_3 \tag{2.3.14}$$

$$\mathrm{Im}\left(\vec{\breve{v}} \cdot \vec{k}\right) = \mathrm{Im}(\breve{u}_1)k_1 + \mathrm{Im}(\breve{u}_2)k_2 + \mathrm{Im}(\breve{u}_3)k_3 \tag{2.3.15}$$

$$k^2 = k_1^2 + k_2^2 + k_3^2 \tag{2.3.16}$$

The real and imaginary parts of the transformed velocity components are corrected by the statements below.

$$\mathrm{Re}(\breve{u}_1) = \mathrm{Re}(\breve{u}_1) - \frac{k_1}{k^2}\mathrm{Re}\left(\vec{\breve{v}} \cdot \vec{k}\right) \tag{2.3.17}$$

$$\mathrm{Im}(\breve{u}_1) = \mathrm{Im}(\breve{u}_1) - \frac{k_1}{k^2}\mathrm{Im}\left(\vec{\breve{v}} \cdot \vec{k}\right) \tag{2.3.18}$$

$$\mathrm{Re}(\breve{u}_2) = \mathrm{Re}(\breve{u}_2) - \frac{k_2}{k^2}\mathrm{Re}\left(\vec{\breve{v}} \cdot \vec{k}\right) \tag{2.3.19}$$

$$\mathrm{Im}(\breve{u}_2) = \mathrm{Im}(\breve{u}_2) - \frac{k_2}{k^2}\mathrm{Im}\left(\vec{\breve{v}} \cdot \vec{k}\right) \tag{2.3.20}$$

$$\mathrm{Re}(\breve{u}_3) = \mathrm{Re}(\breve{u}_3) - \frac{k_3}{k^2}\mathrm{Re}\left(\vec{\breve{v}} \cdot \vec{k}\right) \tag{2.3.21}$$

$$\mathrm{Im}(\breve{u}_3) = \mathrm{Im}(\breve{u}_3) - \frac{k_3}{k^2}\mathrm{Im}\left(\vec{\breve{v}} \cdot \vec{k}\right) \tag{2.3.22}$$

It is important to realize that the transformed velocity components must be set equal zero if all three wavenumber components are zero. If this action is not taken, a spurious, non-physical mode is left within the transform. This undesirable mode is analogous to a rigid body mode occurring in finite element structural analysis.

The transformed velocity components now represent an incompressible flow field satisfying mass conservation. However, this field is not representative of any particular turbulent spectrum. That is to say, isotropic turbulence has a particular kinetic energy spectrum (when computed versus the scalar wavenumber locus). Since the wavenumber field is defined in terms of a discrete subset of the natural numbers, then it has a well-defined maximum and a finite number of elements. Here, the wavevector is addressed by its modulus squared, a scalar locus. By using (2.3.10), the maximum squared wavenumber is

$$k_{\max}^2 = N_1^2 + N_2^2 + N_3^2 \tag{2.3.23}$$

Not all of the natural numbers between zero and $k_{\max}^2$ represent acceptable wavevectors. For these values of k^2, the kinetic energy is assigned the default value of zero. For valid values of k^2 in (2.3.16), the kinetic energy is computed as follows.

$$E(k^2) = \frac{1}{2}\left(\sum_{k^2=\vec{k}\cdot\vec{k}} \left(\breve{u}^*(\vec{k})\,\breve{u}(\vec{k}) + \breve{v}^*(\vec{k})\breve{v}(\vec{k}) + \breve{w}^*(\vec{k})\breve{w}(\vec{k})\right)\right) \tag{2.3.24}$$

The raw spectrum is obtained by summing the energy over the different wavenumber bands. The different wavenumber bands can be determined by dividing $k_{\max}^2$ by max(N_1,N_2,N_3). In each band, the spectral magnitude is scaled by a factor to achieve the magnitude of an archived spectrum such as Comte-Bellot and Corrsin.[18] This scale factor is directly applied to the transformed velocity coefficient.

The final step in developing an isotropic field is to apply the inverse discrete Fourier transformation to the coefficients derived above. The inverse transformation is written as

$$\vec{u}(n_1,n_2,n_3) = \frac{1}{N_1N_2N_3}\sum_{k_1=1-\frac{N_1}{2}}^{N_1-1}\sum_{k_2=1-\frac{N_2}{2}}^{N_2-1}\sum_{k_3=1-\frac{N_3}{2}}^{N_3-1}\breve{\vec{u}}\,(k_1,k_2,k_3) \cdot \exp[i(k_1n_1 + k_2n_2 + k_3n_3)] \tag{2.3.25}$$

for$0 \le n_i \le N_i - 1, n_i = 1,2,3$. For uniform, Cartesian geometries, this velocity distribution is representative of an isotropic turbulence field.

3.0 TEST PROBLEMS

Due to the myriad of physics involved in turbulent chemistry, phase transitions and atomization for fuel droplets, simulating the combustion process for liquid fuel is highly complex. This complexity is inherent in both computer code development and problem execution and solution. In an attempt to this describe type of simulation in a practical way, a set of test problems is introduced below. In this work, the calorically perfect gas equation of state is utilized for the

test problems.

3.1 Gas Phase Acetylene Combustion

This problem is designed to illustrate gas phase combustion; no liquid droplets are involved. Still, the scenario is of practical interest for the field of fuel storage safety. Acetylene is a highly reactive, explosive fuel commonly used as a welding gas. Since it is a gaseous substance at atmospheric temperature and pressure, it must be stored in pressurized tanks. Should this type of tank rupture, the pressurized contents may ignite. A simplified version of this problem can be simulated by defining an air-acetylene distribution near a solid surface. The distribution of species is designed to vary from a premixed gas volume at the exterior of the distribution to the diffusion gas volume near the distribution core. The species involved in this problem are: C_2H_2 (acetylene), N_2 (nitrogen), O_2 (oxygen), Ar (argon), CO_2 (carbon dioxide) and H_2O (water). The single step reaction mechanism presented in equation (2.1.1) is applied here. Naturally, nitrogen and argon are non-reactive species, but since they have noticeable mass fractions in air, they are included to make the mixing problem more realistic. The mass fractions for the species in dry air are presented in Table 2.

Table 2. Mass Fractions of Chemical Species in Air

N_2	O_2	Ar	CO_2
0.7552	0.2314	0.0129	0.0005

The computational domain is box-shaped 10 meters long by 10 meters wide. In terms of height, the vertical domain is stretched in the region above 5 meters to accommodate an expanding cloud. The computational grid is comprised of 48 blocks; each block has 20 cells in each of three directions. The fuel cloud is centered at $x = z = 5$ meters; $y = 0$. The acetylene, nitrogen and oxygen mass fractions are described by a Gaussian distribution applied to the acetylene mass fraction. The relative mass fractions of nitrogen and oxygen match those in air. The mass fraction of acetylene is given by

$$Y_{C_2H_2}(\vec{x}) = \exp\left(\frac{(\vec{x}-\vec{x}_{\text{cen}})^2}{\sigma^2}\right) \quad (3.1.1)$$

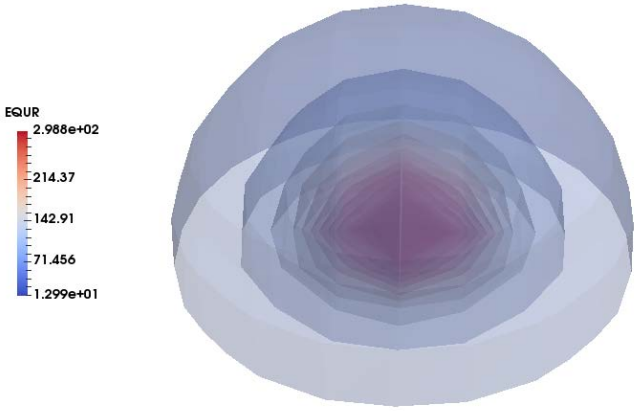

Figure 2. Iso-surfaces of the equivalence ratio for the initial acetylene distribution (oblique view)

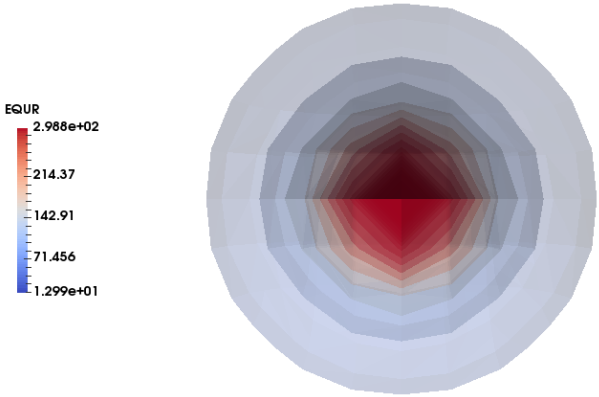

Figure 3. Iso-surfaces of the equivalence ratio for the initial acetylene distribution (overhead view)

where $\vec{x}_{\text{cen}}$ contains the fuel cloud center coordinates, and $\vec{x}$ is a point in the domain. For this case, the width of the Gaussian is implicitly defined by the parameter σ. For this study, σ is set equal one. An equivalence ratio distribution can be computed for the acetylene-air cloud. For the initial conditions, iso-surfaces of the equivalence ratio are shown in Figure 2. An oblique view is shown here. A symmetric view from above is shown in Figure 3. The combustion reaction is initiated by placing a high temperature distribution within the computational domain. This distribution is also Gaussian in the form of (3.1.1) with $\sigma = 0.25$. The center of the distribution is shifted to the coordinates $x = z = 3.75$; $y = 0$. This configuration is easily simulated with LESLIE3D; the LES and EBU algorithms are activated for turbulent combustion. The EBU case is mixing dominated with comparably slow reaction progress. Iso-surfaces of equivalence ratio are shown for this problem at 0.83 seconds in Figure 4 and compared with the initial equivalence

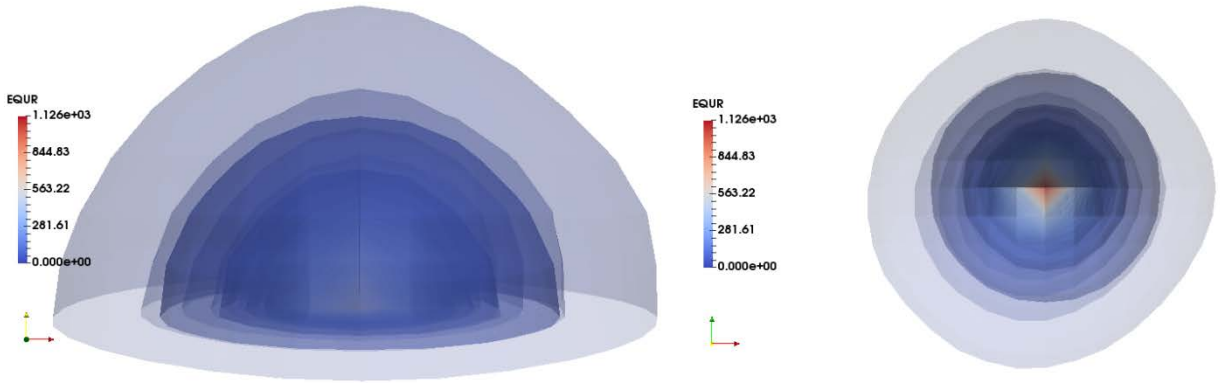

Figure 4. Iso-surfaces of equivalence ratio for the acetylene distribution at 0 and 0.83 seconds (EBU model)

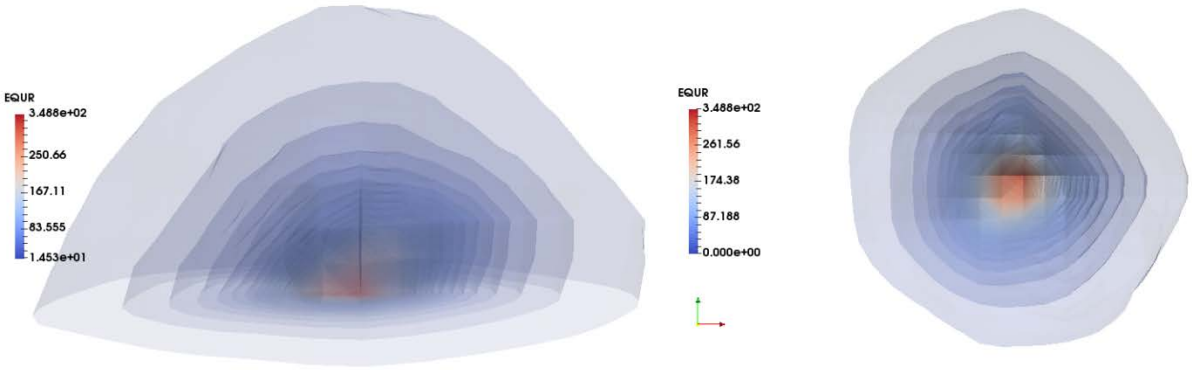

Figure 5. Iso-surfaces of equivalence ratio for the acetylene distribution at 6.36 seconds (EBU model)

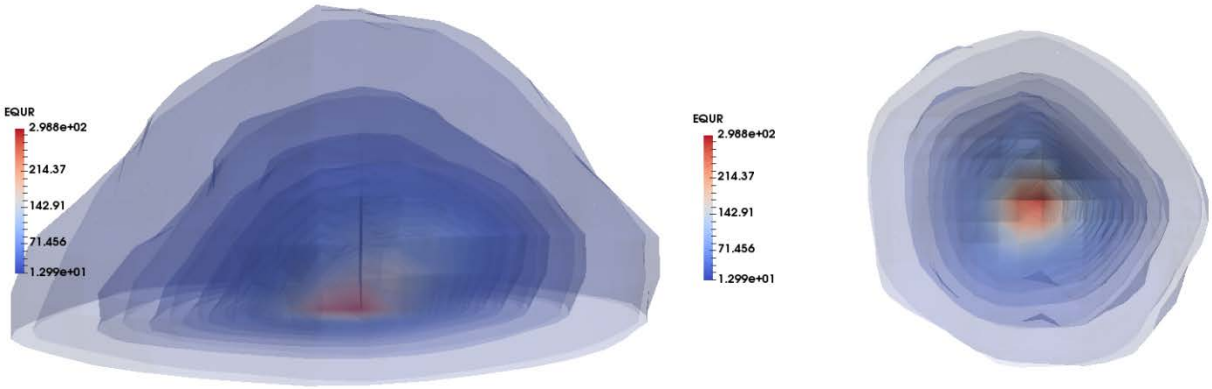

Figure 6. Iso-surfaces of equivalence ratio for the acetylene distribution at 9.53 seconds (EBU model)

ratio. It is evident that the gas volume is moving outward radially, and the fuel density is lowering as is evidenced by the falling equivalence ratio. Peculiarities in the turbulent flow field cause the burn front to evolve with an odd shape. This effect is shown in Figure 5 at 6.36 seconds and in Figure 6 at 9.53 seconds. As is exhibited in Figures 7 through 9, the evolution of the temperature field is more interesting. Turbulent motions are evident through the motion of

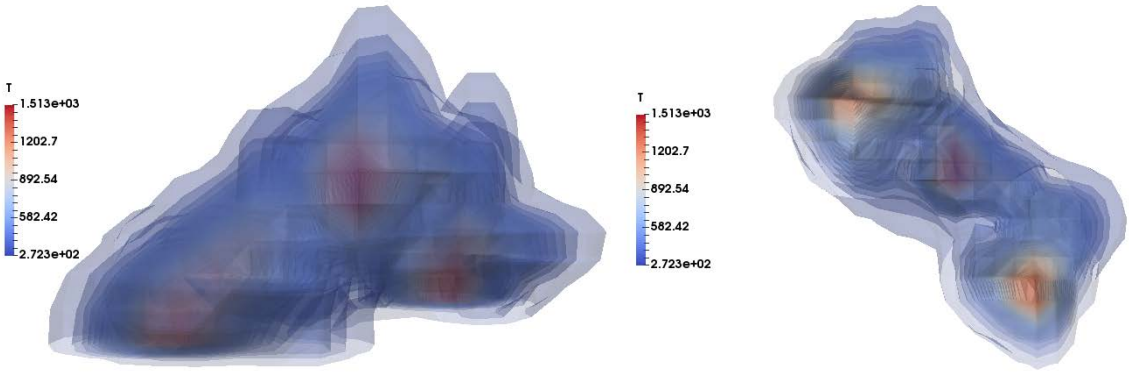

Figure 7. Iso-surfaces of temperature for acetylene combustion at 0.83 seconds (EBU model)

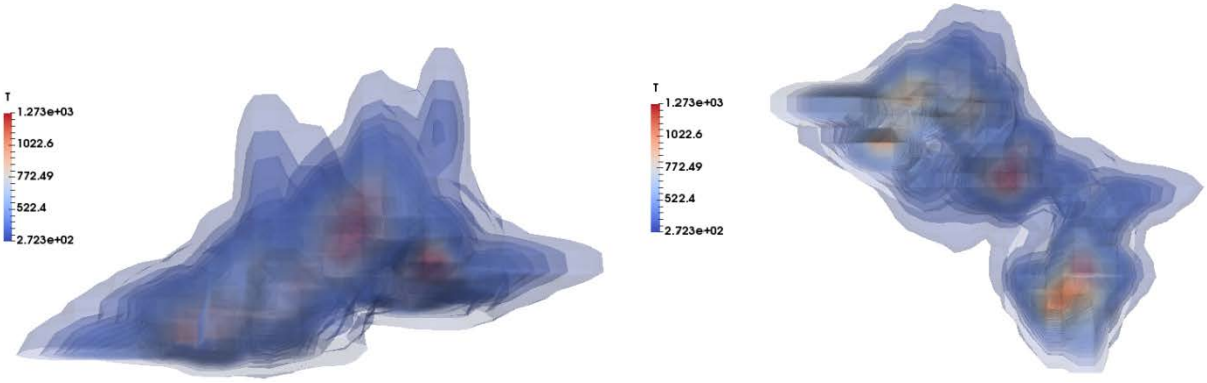

Figure 8. Iso-surfaces of temperature for acetylene combustion at 2.01 seconds (EBU model)

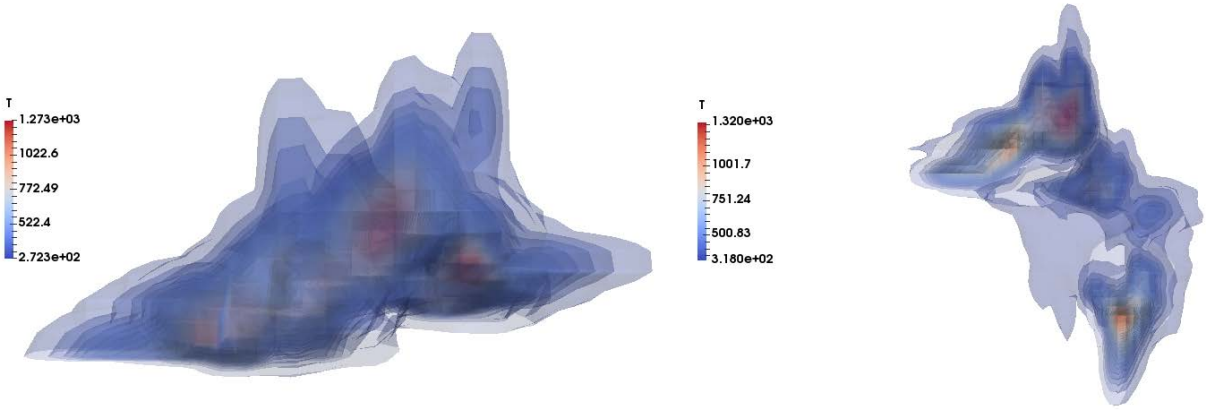

Figure 9. Iso-surfaces of temperature for acetylene combustion at 9.53 seconds (EBU model)

the flame front in this sequence of plots. Although the burn is initiated at single point, it does not spread in a uniform radial directory. Perturbations in the flow field caused by the turbulence split the flame into parts that propagate in different directions. Although the burn is more intense near the point of initiation, it also develops two distinct lobes when viewed from above and takes on

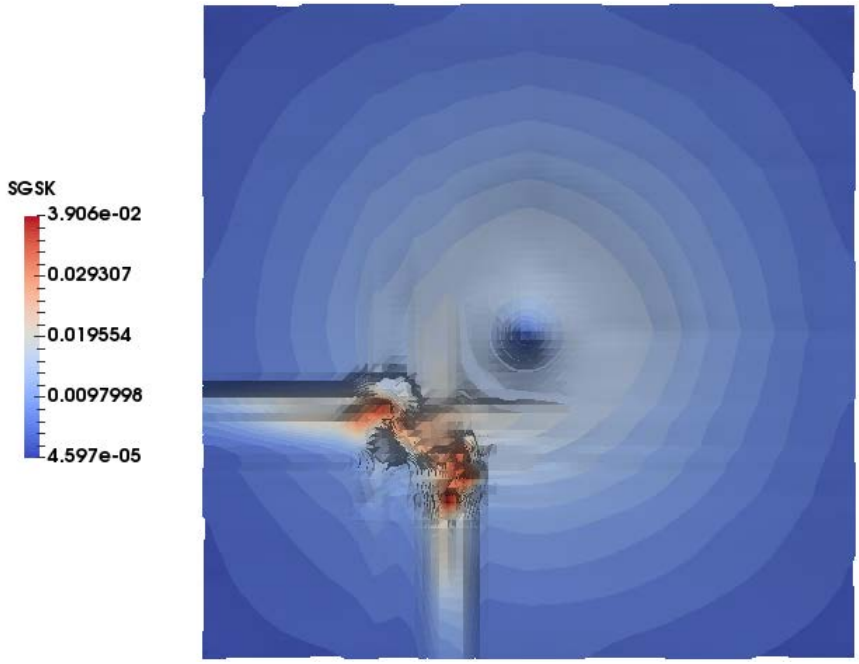

Figure 10. Iso-surface plot of subgrid kinetic energy at 9.53 seconds

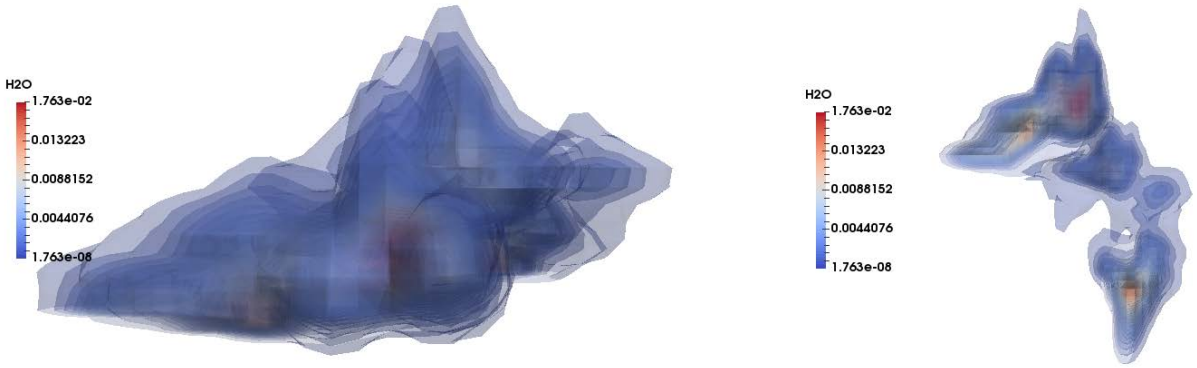

Figure 11. Iso-surface plot of water mass fraction at 9.53 seconds

the shape of a bow. The flame spreads laterally but unevenly for this reason as is evident in Figures 7, 8 and 9. The spatial extent of the flame correlates well with the distribution of subgrid kinetic energy. One may see this correlation by comparing Figures 9 and 10. Figure 10 contains an iso-surface plot of subgrid kinetic energy viewed perpendicular to the *y* axis. Due to the lack of grid refinement used in the case, the turbulent wall interactions are over predicted. Still, the correlation between the combustion reaction and subgrid kinetic energy is well illustrated. A view of product formation is also provided by the numerical solution and shown in Figure 11. The concentration of water closely follows the temperature and subgrid kinetic energy

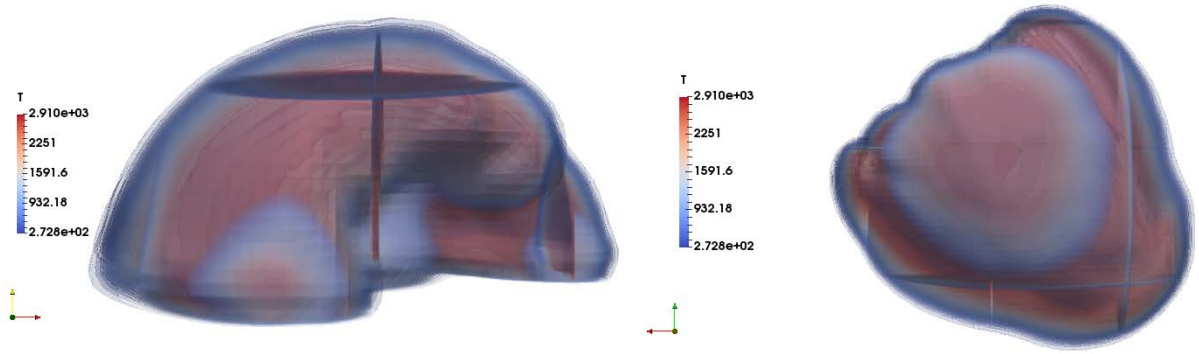

Figure 12. Iso-surface plots of temperature at 0.05 seconds (kinetic model)

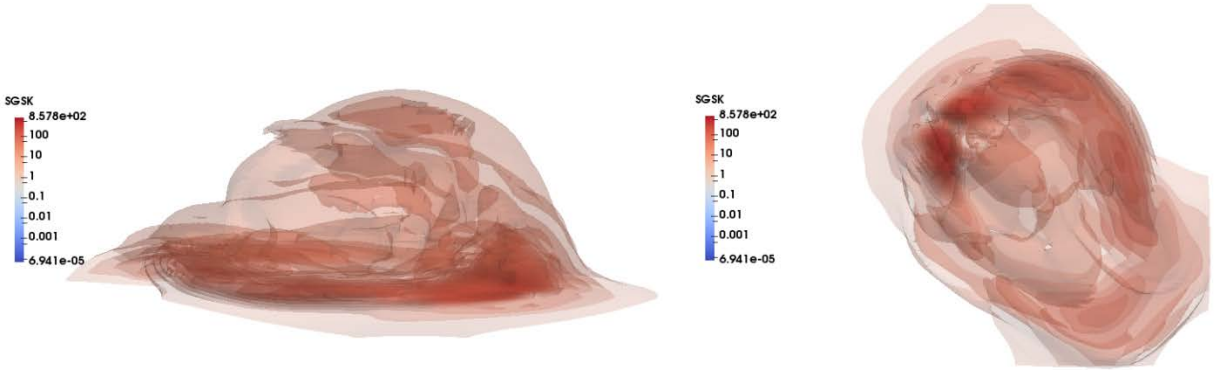

Figure 13. Iso-surface plots of subgrid kinetic energy at 0.07 seconds (kinetic model)

distributions. The reaction is driven by the chemical rate (represented by temperature) and by turbulent mixing (represented by subgrid kinetic energy).

It is interesting to contrast the results of the EBU model with those associated with is referred to here as the kinetic model. For the kinetic model, the reaction rates produced by the chemical mechanism are chosen as the actual reaction rates. No turbulent closure is applied to the chemical rates. As a result, reactants found within a grid cell are assumed to be fully mixed and react to the fullest extent dictated by the kinetic mechanism. Figures 12 and 13 shown the results for temperature at 0.05 seconds and for subgrid kinetic energy at 0.07 seconds, respectively, for this model. Turbulence still has an effect on the overall distribution of properties, but it is less pronounced since it has less of an effect on local reaction rates. The kinetic model can over predict reaction rates by neglect turbulent mixing. Under the kinetic model, reactions proceed more rapidly. This effect is illustrated by Figure 14, a comparison of the temperature distribution for the kinetic model at 0.05 and 0.07 seconds. The different temperature distributions can be identified by the blue lines. It is evident that the blast cloud

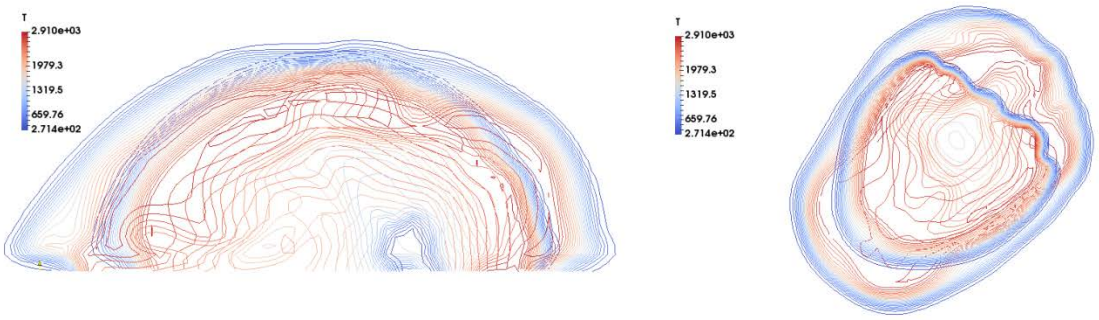

Figure 14. Temperature contours for the kinetic model at 0.05 and 0.07 seconds

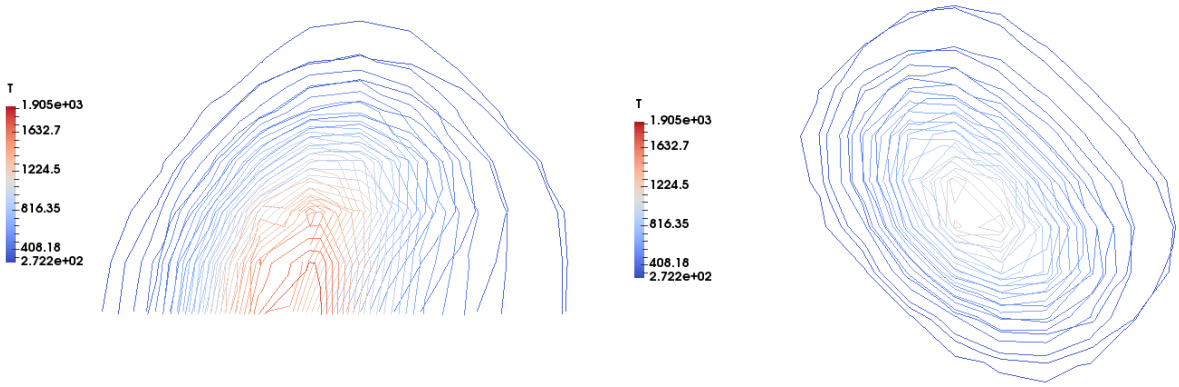

Figure 15. Temperature contours for the EBU model at 0.04 and 0.07 seconds

expands significantly in the span of 0.02 seconds. A similar plot is provided for the EBU model in Figure 15. The temperature contours closely plot over one another in this with 0.03 seconds between the temperature solutions. The kinetic solution advances faster than the EBU solution.

3.2 Kerosene Droplet Combustion

The acetylene burn problem discussed in Section 3.1 is fundamental in that it entails the combustion of a purely gaseous substance. Acetylene is a purely gaseous substance in this case, so no phase change is involved. A more common occurrence entails the release of fuel in droplet form; under the right thermal conditions, the droplets break down and vaporize. The portion of the fuel now in the gas phase can combust transforming into reaction products. The test fuel considered here is kerosene, a principal component of jet fuel. This problem is more interesting and complex than the preceding test case because kerosene is not a pure substance; rather, it is mixture of alkanes (like heptane), naphthenes (or cyclo-alkanes, like cyclobutane), alkenes (like ethylene) and aromatic hydrocarbons (like benzene).[19] Secondly, the evaporation phase change and subsequent vapor ignition is caused by the impact of a series of incident and reflected shock waves

inside of a square shock tube.[20] Heating of the droplets, in this situation, requires hydrodynamic compression of the gas with the increase in temperature predicted by the equation of state. The repetition of archived experiments via simulation is also complicated by the fact that in many experiments, the initial conditions in the shock tube, (e.g., pressures in the driver and driven sections) are not documented. Experimentalists often concentrate on achieving a particular pressure behind the reflected shock wave.[21] The task of replicating this pressure in the simulation set-up is left to the computational physicist.

Given the time allowed for accomplishing this report, a simplified problem involving the shock tube ignition of kerosene droplets is described. The shock tube has a square cross-section that is one meter in width by one meter in height. The tube length is 48 meters, and the driver section is 16 meters long (1/3 of the tube length). To generate a reflected shock wave, the driven end of the tube is terminated with a solid surface. Each one meter section of tube length is designated as a subdomain (or block). Each block is uniformly meshed with 20 cells in each of the three Cartesian directions. The field of 20,000 kerosene droplet parcels is suspended between locations 24 and 33.6 meters along the length of the shock tube. Each parcel consists of 100 droplets. The particle radii are randomly selected to be between 37.5 μm and 50.0 μm. The droplet (x, y, z) coordinates are given by the equations

$$\begin{aligned} x_d &= 24.0 + 9.6 \cdot RAND \\ y_d &= \quad 0.2 + 0.6 \cdot RAND \\ z_d &= \quad 0.2 + 0.6 \cdot RAND \end{aligned} \tag{3.2.1}$$

These equations place the droplets at random locations within a box-shaped region within the tube. *RAND* is a series of sequentially generated pseudorandom numbers used to place the droplets at random locations. By using this process, we avoid creating a Cartesian array of droplets. Also, the droplets are assigned small, random initial velocities (magnitude 0.1 m/s) since most experiments inject droplets into the shock tube with some initial velocity.

LESLIE3D contains a model for evaporation that draws upon a thermochemical properties file for kerosene. As a result, this computer program can simulate the evaporation of kerosene droplets. As the droplets begin to evaporate into kerosene vapor, finite rate chemistry algorithms are invoked to burn the kerosene into products. A simplified version of the reduced reaction kinetics model developed by Franzelli et al. [22] is employed to capture the chemistry in conjunction with the EBU turbulent closure model. This mechanism, consisting of two steps, is very efficient for numerical applications. It is written as

$$(1)\ C_{10}H_{20} + 10\ O_2 \rightarrow 10\ CO + 10\ H_2O \qquad (3.2.2)$$

The second step involves the oxidation of carbon monoxide to for carbon dioxide, i.e.,

$$(2)\ CO + \tfrac{1}{2}\ O_2 \rightarrow CO_2 \qquad (3.2.3)$$

Table 3. Kerosene Combustion Reaction Coefficient Data

Reaction Step	*A*	*n*	*E/R*
1	8×10^{11}	1	4.15×10^{4}
2	4.5×10^{10}	1	2×10^{4}

The rate expressions for reactions (3.2.2) and (3.2.3) are written as follows.

$$r_{f1} = k_1[C_{10}H_{20}]^{0.55}[O_2]^{0.9} \qquad (3.2.4)$$

$$r_{f2} = k_2[CO]^{1}[O_2]^{0.5} \qquad (3.2.5)$$

Correction terms based upon equivalence ratio are applied to the pre-exponential factors in [19]; for simplicity, these factors are not employed here. For the version of LESLIE3D addressed here, the user is required to write the source code for any particular finite rate chemistry mechanism unless such coding is available from an archived source.

Initial conditions within the driver and driven sections of the shock tube are provided in Table 4. A turbulent initial velocity field is also established within the shock tube in accordance with the method described in Section 2.3. The conditions are selected to ensure droplet evaporation and ignition via shock heating. The initial data for both the gas and particle fields is

Table 4. Shock Tube Initial Conditions

Property	**Driver Section**	**Driven Section**
Pressure (Pa)	214967.0	2293.14
Temperature (K)	800.0	300.0

coded *a priori* in initial LESLIE3D restart and droplet files. These files are read by LESLIE3D at time of code execution. By far, the majority of time in conducting this simulation is in setting up the initial data; very little time is required to configure LESLIE3D. On 48 cores, this simulation executes rather quickly, at approximately three seconds per iteration (or step).

Results have been generated for the kerosene droplet burn problem out to 111 milliseconds

(ms) over 7000 iterations. A sequence of temperature field plots is included. Each plot has an overlay of the kerosene droplet field existing at the same time. Figure 16 contains these plots in order at 12 ms, 15 ms, 18 ms, 21 ms, 23 ms and 25 ms. In this figure, note that although the temperature field is shown in translucent coloration, the particle parcels are shown as block dots. During this segment of the numerical solution, kerosene droplet parcels are actively evaporating. LESLIE3D actively provides the parcel count; a sampling of this count is shown in Table 4. With evaporation combined with hydrodynamic and turbulent motion, the

Table 3. Time dependent inventory of kerosene droplet parcels

Time (ms)	12	15	18	21	23	25
Parcels	20,000	18,375	12,641	6,419	1,097	83

gaseous kerosene field evolves. Slice plots of the mass fraction for kerosene are presented in Figure 17 at 12 ms, 15 ms , 18 ms, 21 ms, 23 ms and 26 ms. From this figure one may see that kerosene vapor is formed at the shock outflow and is then advected along with flow field trailing the main shock. By plotting kerosene's mass fraction on the same scale, the accumulation of kerosene (increasing mass fraction) is evident at the shock outflow. Since the droplets are suspended near the tube core, away from the walls, little kerosene vapor accumulates near the tube walls. For this reason, the slice plots are taken along a plane through the tube centerline. Doing so provides a clearer picture of the kerosene vapor distribution. This emission of kerosene vapor motivates the question as to whether it is burning in the tube. An answer to this inquiry is provided by examining the generation of product mass, e.g., for water vapor, within the tube. Recall that for each mole of kerosene burned, the first reaction step generates 10 moles of water and 10 moles of carbon dioxide. Slice plots of the mass fraction of water are shown in Figure 18. It is interesting to compare Figures 17 and 18. The distribution of water vapor closely follows that of kerosene vapor because kerosene is burning producing the water vapor. Both of these gases are advected by the shock outflow; hence, as is shown in these two figures, the gas volumes follow the shock wave. The distribution of carbon monoxide would look very similar since it is produced on a one to one molar ratio with water. Similar statements can be made for the distribution of carbon dioxide in the tube. The mass fraction is about an order of magnitude smaller than that of carbon monoxide its primary reactant.

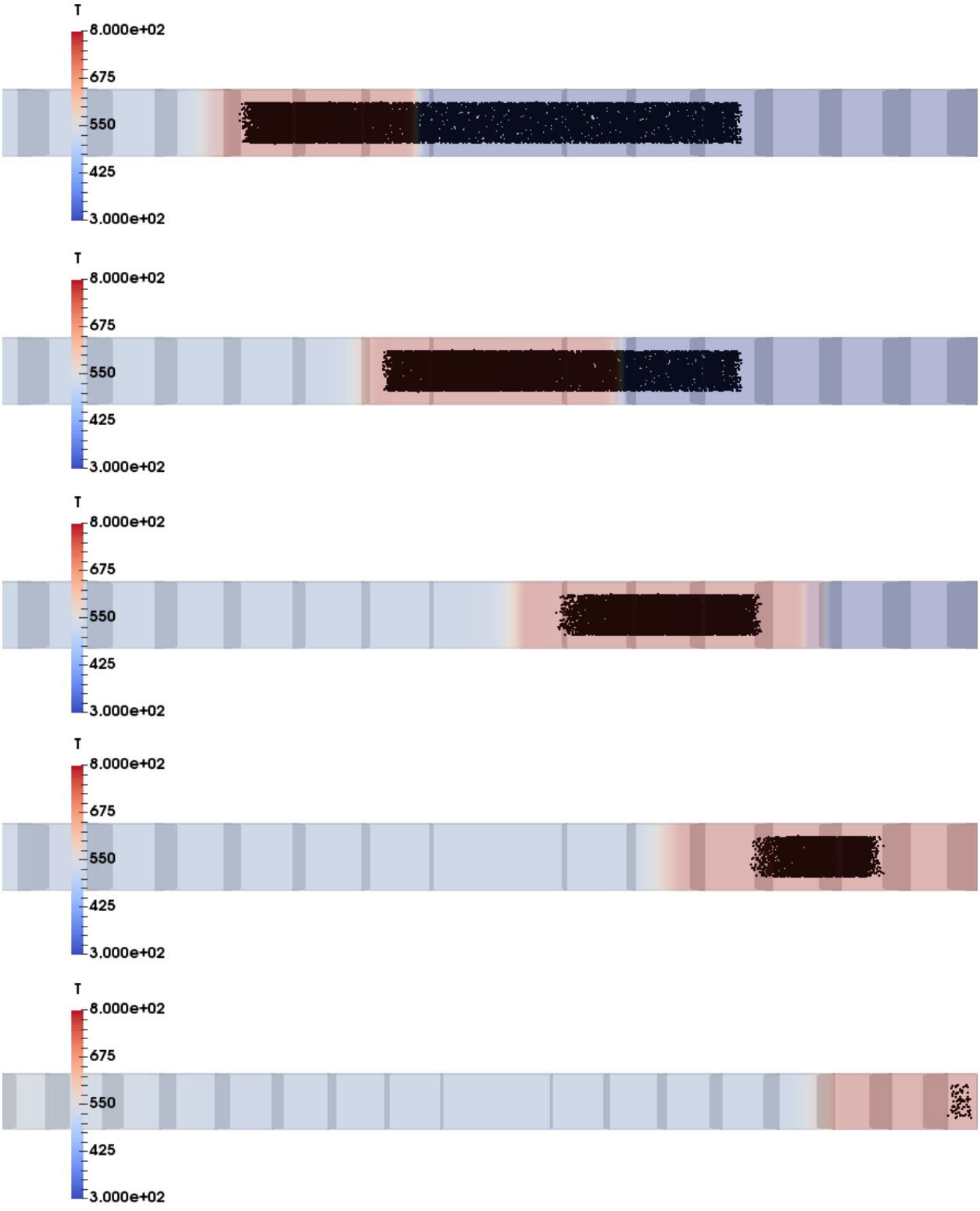

Figure 16. Shock tube temperature plots including particle positions at 12, 15, 18, 21, 23 and 25 milliseconds

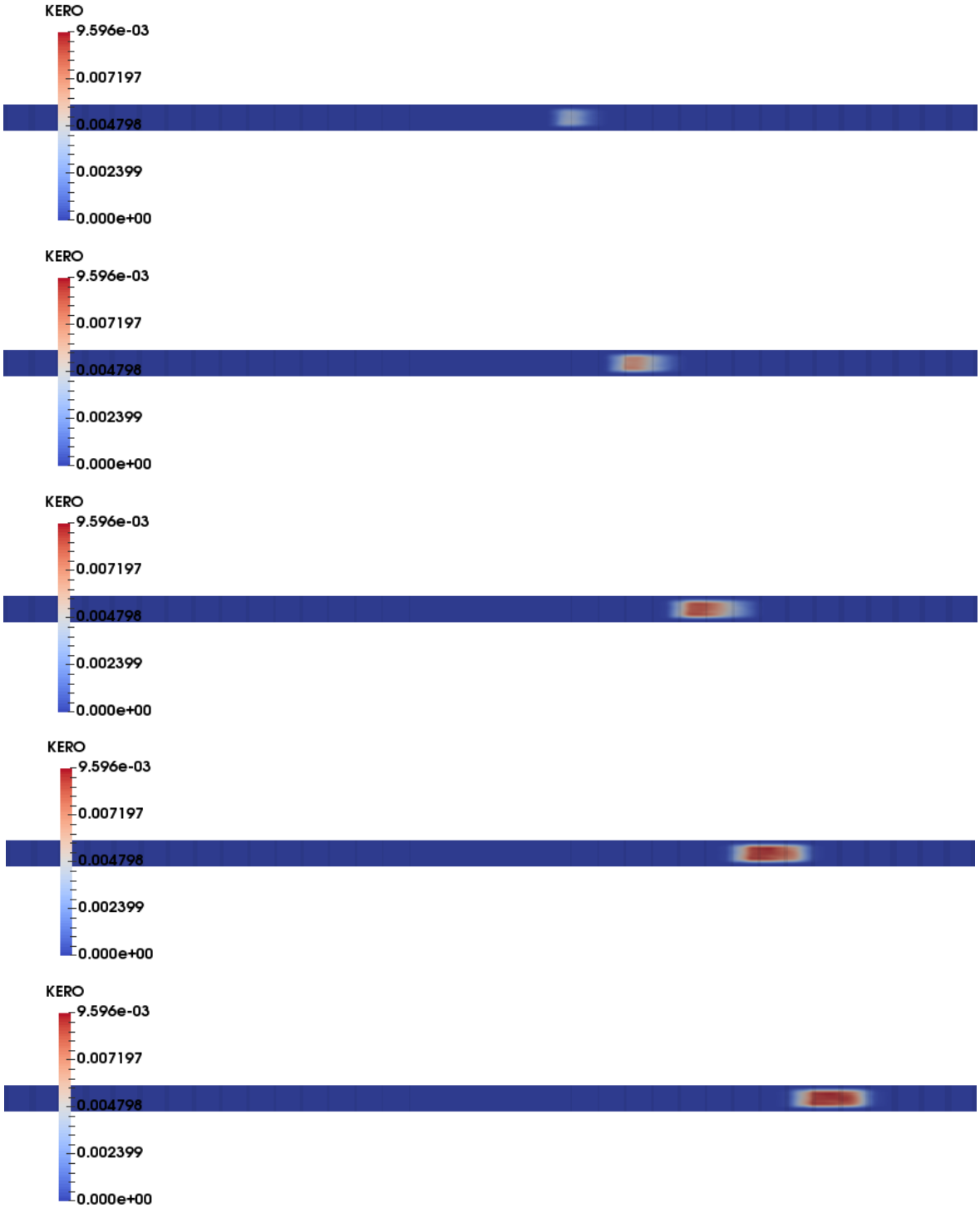
KERO
9.596e-03
0.007197
0.004798
0.002399
0.000e+00
KERO
9.596e-03
0.007197
0.004798
0.002399
0.000e+00
KERO
9.596e-03
0.007197
0.004798
0.002399
0.000e+00
KERO
9.596e-03
0.007197
0.004798
0.002399
0.000e+00
KERO
9.596e-03
0.007197
0.004798
0.002399
0.000e+00

Figure 17. Slice plots of kerosene vapor mass fraction at 12, 15, 18, 21, 23 and 26 milliseconds

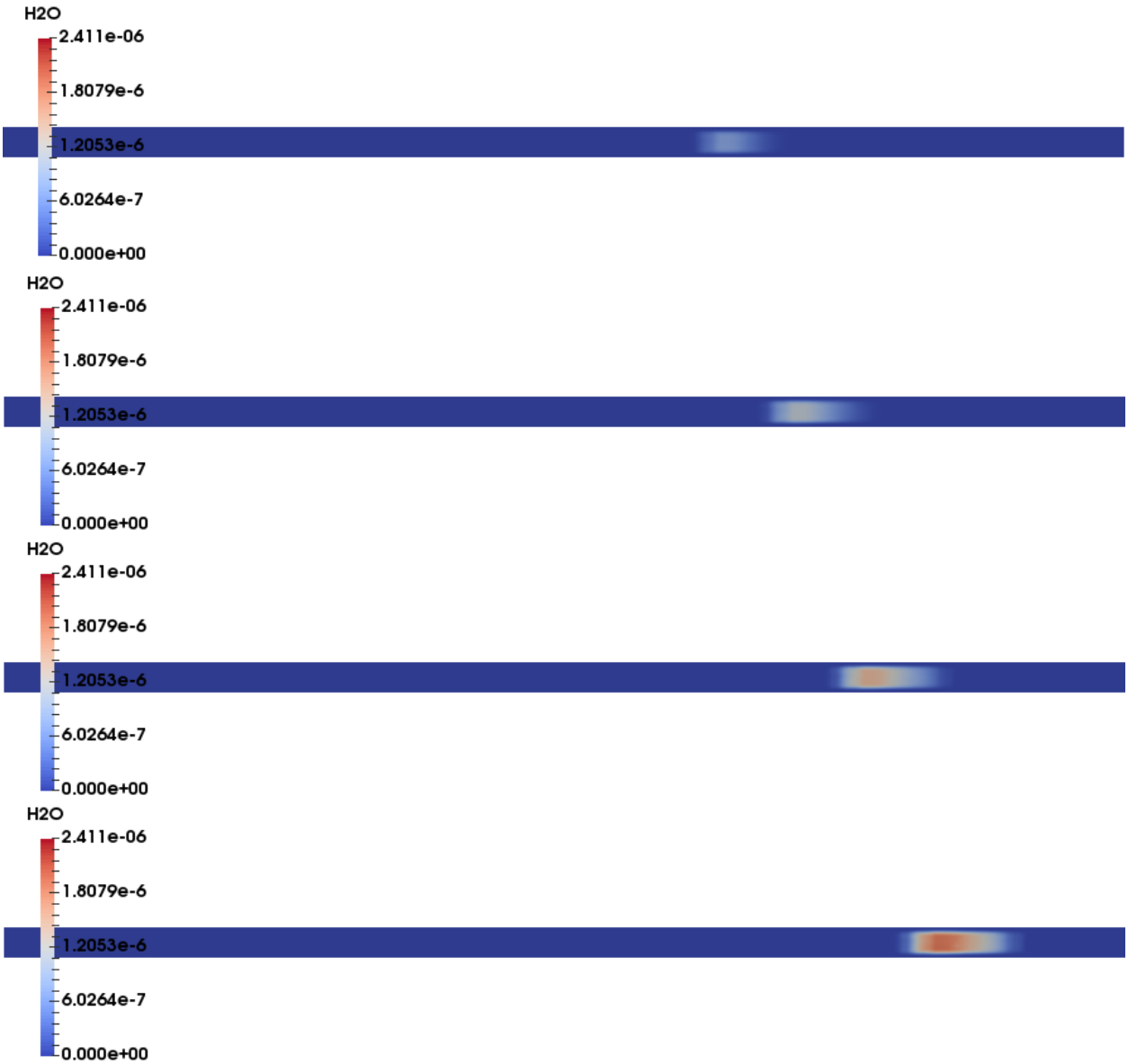

Figure 18. Slice plots of water vapor mass fraction at 15, 18, 21, 23 and 26 milliseconds

4.0 CONCLUSIONS

This technical memorandum documents continued progress in assimilating the LESLIE3D multiphase physics computer program for applications in shocked reactive flow fields. As an expository work, this memorandum concentrates on describing LESLIE3D's turbulent finite rate chemistry algorithms. The term "turbulent" is used for two reasons. In the first place, LESLIE3D incorporates state-of-the-art algorithms for the large eddy simulation of compressible turbulence. Secondly, the code applies turbulent chemical closures to incorporate the physical limitations of reaction rates imposed by mixing. The simplest example of the turbulent chemical closure is the Eddy Break-Up model described herein. The effect of this closure is illustrated by the acetylene combustion problem. The evolution of the acetylene burn is compared with and without this closure. Results show that the combustion reaction proceeds much more quickly for the kinetic model. This model does not use a turbulent closure; rather in each cell, perfect mixing is assumed for the reactants. When the Eddy Break-Up model is employed, the reaction proceeds more slowly. Since perfectly mixing rarely occurs in the real world, we expect the kinetic model to overestimate chemical reaction rates. This assertion has important ramifications for a number of different engineering fields.

A second topic addressed by this memorandum is the evaporation and subsequent combustion of liquid fuel droplets. Kerosene, a complex hydrogen mixture, is explored from the standpoint of shock-initiated combustion. LESLIE3D simulates the evaporation of a wide distribution of droplet diameters and then applies a finite rate chemical mechanism to simulate kerosene combustion. A related fact is that LESLIE3D can simulate chemical mechanisms involving an arbitrary number of species and reaction steps known *a priori* (limited only by

computer memory). In this work, a simplified adaptation of the mechanism developed by Franzetti et al. is employed. The simulation results show the time dependent evaporation of kerosene (as modeled) and its transformation into products. The positions and velocities of the droplets are predicted by LESLIE3D in the Lagrangian sense. The successful completion of this problem constitutes a highly applicable framework for solving an array of problems involving the combustion of fuel or in the wider view, the consumption of an arbitrary reactant. Time permitting, more complex models may be constructed and solved to elucidate important aspects of chemical physics.

REFERENCES

1. Sankaran, V. and Menon, S., LES of spray combustion in swirling flows, *Journal of Turbulence,* Vol. 3, No. 1, 2002, pp. 011.

2. Lesieur, M., *Turbulence in Fluids,* 2nd Revised Ed., Fluid Mechanics and Its Applications, Vol. 1, Kluwer Academic Publishers, Boston, Massachusetts, 1990.

3. Genin, F. *Study of Compressible Turbulent Flows in Supersonic Environment by Large-Eddy Simulation.* Doctoral Dissertation, Georgia Institute of Technology, 2009.

4. Erlebacher, G., Hussaini, M.Y., Speziale, C.G. and Zang, T.A., "Toward the large-eddy simulation of compressible flows", *Journal of Fluid Mechanics,* Vol. 238, 1992, pp. 155-185.

5. Hirsch, C., *Numerical Computation of Internal and External Flows, Vol. 2, Computational Methods for Inviscid and Viscous Flows.* John Wiley & Sons, New York, NY, 1990.

6. Collela, P. and Woodward, P., "The piece-wise parabolic method for hydrodynamics", *Journal of Computational Physics*. Vol. 54, pp. 174-201, 1984.

7. Harten, A., Lax, P.D. and van Leer, B., "On upstream differencing and Godunov-type schemes for hyperbolic conservation laws", *SIAM Review,* Vol. 25, pp. 35-61, 1983.

8. Einfeldt, B., "On Godunov-type methods for gas dynamics", *SIAM Journal of Numerical Analysis.* Vol. 25, No. 2, pp. 294-318, 1988.

9. Balakrishnan, K., Nance, D.V. and Menon, S., "Simulation of impulse effects from explosive charges containing metal particles", *Shock Waves,* Vol. 20, No. 3, 2010, pp. 217-239.

10. Carlson, D.J. and Hoglund, R.F., "Particle drag and heat transfer in rocket nozzles", *AIAA Journal*, Vol. 2, No. 11, 1964, pp. 1980-1984.

11. Makhviladze, G.M. and Yakush, S.E., "Modelling of fires following bursts of pressurized fuel tanks", *Proceedings of the 7th International Symposium on Fire Safety Science*, 2003, pp. 643-654.

12. Makhviladze, G.M. and Yakush, S.E., "Modelling of formation and combustion of accidentally released fuel clouds", *Process Safety and Environmental Protection*, Vol. 83, No. 2, 2005, pp. 171-177.

13. Westbrook, C.K. and Dryer, F.L., "Simplified reaction mechanisms for the oxidation of hydrocarbon fuels in flames", *Combustion Science and Technology*, Vol. 27, 1981, pp. 31-43.

14. Spalding, D.B., "Development of the Eddy Break-Up model for turbulent combustion", *16th International Symposium on Combustion*, The Combustion Institute, 1976, pp. 1657-1663.

15. Poinsot, T. and Veynante, D., *Theoretical and Numerical Combustion.* R.T. Edwards, Inc., Philadelphia, Pennsylvania, 2001.

16. Knight, D., Zhou, G., Okong'o, N. and Shukla, V., "Compressible large eddy simulation using unstructured grids", AIAA Paper 98-0535, 1998.

17. L'Ecuyer, P., "Uniform Random Number Generation", *Annals of Operations Research*, Vol. 53, 1994, pp. 77-120.

18. Comte-Bellot, G. and Corrsin, S., "Simple Eulerian time correlation of full- and narrow-band velocity signals in grid-generated, isotropic turbulence", *Journal of Fluid Mechanics*, Vol. 48, 1971, pp. 273-337.

19. Wang, T.-S., "Thermophysics characterization of kerosene combustion", *Journal of Thermophysics and Heat Transfer*, Vol. 15, No. 2, 2001, pp. 140-147.

20. Char, J.M., Liou, W.J., Yeh, J.H. and Chiu, C.L., "Ignition and combustion study of JP-8 fuel in a supersonic flowfield", *Shock Waves*, Vol. 6, No. 5, 1996, pp. 259-266.

21. Rotavera, B. and Petersen, E.L., "Atomized fuel combustion in the reflected-shock region", *Shock Waves - 26th International Symposium on Shock Waves.* Vol. 1, Hanneman, K. and Seiler, F., Eds., Springer, New York, New York, 2009, pp. 141-146.

22. Franzelli, B., Riber, E., Sanjose, M. and Poinsot, T., “A two-step chemical scheme for kerosene-air premixed flames”, *Combustion and Flame*, Vol. 157, No. 7, 2010, pp. 1364-1373.

DISTRIBUTION LIST
AFRL-RW-EG-TP-2016-002

*Defense Technical Info Center
8725 John J. Kingman Rd Ste 0944
Fort Belvoir VA 22060-6218

AFRL/RWML (1)
AFRL/RWORR (STINFO Office) (1)